

Tripartite State Characterization via Activated Bipartite Entanglement

L. G. E. Arruda,^{1,*} W. F. Balthazar,^{2,3,†} M. V. Moreira,^{1,‡} M. H. M. Passos,^{4,§} J. A. O. Huguenin,^{5,6,¶} and M. C. de Oliveira^{1, **}

¹*Instituto de Física Gleb Wataghin, Universidade de Campinas, 13083-970, Campinas, SP, Brazil*

²*Instituto Federal de Educação, Ciência e Tecnologia do Rio de Janeiro - IFRJ, Volta Redonda, RJ, Brazil*

³*Programa de Pós-graduação em Física, Instituto de Física, Universidade Federal Fluminense, Niterói, RJ, Brazil*

⁴*ICFO—Institut de Ciències Fotoniques, the Barcelona Institute of Science and Technology, 08860 Castelldefels (Barcelona), Spain*

⁵*Instituto de Ciencias Exatas, Universidade Federal Fluminense, Volta Redonda, RJ, Brazil*

⁶*Programa de Pós-graduação em Física, Instituto de Física, Universidade Federal Fluminense, Niterói, RJ, Brazil*

(Dated: June 8, 2022)

We propose a way to identify and classify genuine tripartite entanglement in pure states of three-qubit systems via the Activated Bipartite Entanglement (ABE). We show that for pure states pertaining to one of the two inequivalent classes of genuine tripartite entanglement, for which the GHZ and the W states are the notorious representatives, the ABE is always greater than zero, while for separable tripartite pure states or bipartite entanglement between two parts of three-qubit pure states it is always null. In addition we present a experimental proposal by using liner optical circuits and degrees of freedom of a single photon to verify the characterization via distributed entanglement. The circuit simulation showed an excellent accordance with theoretical prediction for a wide classes of GHZ states.

PACS numbers: VERIFICAR PACS NUMBERS

I. INTRODUCTION

After decades of theoretical and experimental research, entanglement has gained the status of a fundamental non-local resource, necessary to accomplish informational tasks in a more efficient way than in classical systems. While bipartite entanglement is well understood and properly quantified for arbitrarily mixed states, for both discrete [1] and continuous variable [2], the entanglement of multipartite composite systems has been a challenge to be quantitatively and qualitatively well characterized [3]. In principle, two different approaches can be used to quantify entanglement – an operational and an abstract (axiomatic) [4, 5]. The first one is related to operational tasks – the system is more entangled if it allows for better performance on a certain task. In the second approach, a state function can be used to quantify entanglement if it satisfies some reasonable properties. A good measure of entanglement should capture its essential characteristics and should ideally be related to an operational procedure. Depending on the purpose, a variety of different properties may be required [5].

The quality of some fixed amount of entanglement present in combined systems might be linked with the inequivalent classes of entanglement that they belong to. For multipartite systems, there are more than one inequivalent class of entanglement, giving rise to a classification of entangled states based on the impossibility to transform one state belonging to a specific class into a state belonging to another class through local operations and classical communication (LOCC). The

two prominent classes of genuinely tripartite entangled states, for instance, are the W class and GHZ class [6]. The extension for multipartite systems of larger dimensions is desirable, but difficult to be foreseen, although some previous attempts have been given [7–9]. Despite all the previous effort, the attempt to define a single entanglement measure that would capture the essence of the distinct classes has been unsuccessful.

In this paper, we propose a way to distinguish quantitatively if a pure three-qubit state, ρ_{ABC} , presents a genuine tripartite entanglement or not through the difference between the posterior and anterior localized bipartite entanglement of state ρ_{AB} , in respect to the actuation in C . As it turns out, this measure, here called Activated Bipartite Entanglement (ABE), is simply characterized by the difference between two dual entanglement measures, the Entanglement of Assistance (EoA) [10] and the Entanglement of Formation (EoF) [11]. The ABE distinguishes if some tripartite pure state possesses a genuine tripartite entanglement or if it possesses only a bipartite entanglement between or even no entanglement at all. It also allows for a clear ordering of states in a parameter map, where it is possible to distinguish all classes of entanglement.

To illustrate the applicability of the ABE, we present a proposal for the generation of GHZ-type and W-type tripartite states, employing linear optics. Linear optical circuits are very precise and an excellent test bed for entanglement studies [12]. They have been used, for instance, for the implementation of the sudden death entanglement induced by environments emulated by linear transformations of polarization of twin-photons [13], by polarization mode dispersion [14] and by an all-optical local CNOT [15]. Internal degrees of freedom of twin-photons were explored for preparation and geometry study of GHZ states [16]. A 18-qubit GHZ entangled state was prepared by simultaneous exploiting path, polarization, and orbital angular momentum (OAM) of six photons produced by three Spontaneous Parametric Down Conversion (SPDC) with very good fidelity [17]. By using these three degrees of freedom of single photons, it was previously

* lgarruda@ifi.unicamp.br

† wagner.balthazar@ifrj.edu.br

‡ mvaxs@ifi.unicamp.br

§ marcello.passos@icfo.eu

¶ jose_huguenin@id.uff.br

** marcos@ifi.unicamp.br

proposed a full linear optical circuit to prepare tripartite GHZ state [18, 19]. Here, also using path, polarization, and OAM we propose an experiment exploring the detection of ABE for the classes of GHZ and W states.

In what follows, we will discuss some concepts, definitions, and results concerning the entanglement between parts of a composite system that will be important for the understanding of our work. The paper is organized as follows. In Sec. II, we review the definition of Entanglement of Assistance and Entanglement of Formation. In Sec. III, we define the Activated Bipartite Entanglement measure. We discuss an application of the Activated Bipartite Entanglement for the characterization of the entanglement between three qubits, through a numerical, and exact approach in Secs. IV and V, respectively. In Sec. VI we present and experimental proposal in terms of linear optical devices and discuss the simulated results. Finally, in Sec. VII a conclusion encloses the paper.

II. ENTANGLEMENT OF ASSISTANCE

The definition of the Entanglement of Assistance (EoA) [10] is motivated by the situation in which three parties spatially separated, let us say Alice, Bob, and Charlie (ABC), share many copies of a tripartite pure entangled state given by $\rho_{ABC} = |\psi_{ABC}\rangle\langle\psi_{ABC}|$, and Alice and Bob (AB) would like to use their subsystems to perform some particular task. However, the reduced state shared by AB, $\rho_{AB} = \text{Tr}_C [\rho_{ABC}]$, might not be very pure nor sufficiently entangled for this purpose. Charlie (C) is not able to physically transfer his subsystem to one of them. On the other hand, he can effectively help them by remotely transforming the available resource by doing appropriate local projective measurements in his subsystem. This procedure concentrates the initial tripartite entanglement in a new set of bipartite copies, shared by AB. This bipartite entangled state will be conditioned to the local projective measurements done by C. For that, C has to find the best basis to perform his projective measurements such that it maximizes the entanglement of the copies shared by AB. Let us suppose a measurement that creates pure states $|\psi_{AB}^i\rangle$ with probabilities p_i , then the rate that AB can convert their new states into singlets to perform their task is given by [20]

$$\bar{S}(\varepsilon) = \sum_i p_i S(\rho_A^i) = -\sum_i p_i \text{Tr}(\rho_A^i \log \rho_A^i), \quad (1)$$

where $\varepsilon = \{p_i, \rho_{AB}^i\}$ represents the ensemble made up of pure states $\rho_{AB}^i = |\psi_{AB}^i\rangle\langle\psi_{AB}^i|$. The EoA is defined as the maximization of the conversion rate given by Eq. (1) over all convex decompositions of ρ_{AB} into pure states, that is, over all ensembles ε which $\rho_{AB} = \sum_i p_i |\psi_{AB}^i\rangle\langle\psi_{AB}^i|$. Thus, the EoA is given by

$$E_A(\rho_{AB}) = \max_{\varepsilon} \bar{S}(\varepsilon) = \max_{\{p_i, \rho_{AB}^i\}} \sum_i p_i S(\rho_A^i). \quad (2)$$

It is important to note that the EoA is dual to the Entanglement of Formation (EoF) between Alice and Bob alone

($\rho_{AB} = \text{Tr}_C \rho_{ABC}$), as it is defined as the minimum value of the average entropy $\bar{S}(\varepsilon)$ over all possible pure state decomposition of ρ_{AB} [11],

$$E_F(\rho_{AB}) = \min_{\varepsilon} \bar{S}(\varepsilon) = \min_{\{p_i, \rho_{AB}^i\}} \sum_i p_i S(\rho_A^i). \quad (3)$$

Note that the EoF captures the amount of entanglement of the pair AB, irrespective to C. Although the EoA captures the amount of entanglement that is localized in the pair AB with the assistance of C, it does not distinguish whether ρ_{AB} was previously entangled or not.

To apply Eq. (2) in some concrete examples, let us consider an arbitrary orthonormal basis to accomplish the projective measurements

$$\begin{aligned} |\xi\rangle &= \cos \theta |0\rangle_C + e^{i\phi} \sin \theta |1\rangle_C, \\ |\chi\rangle &= \sin \theta |0\rangle_C - e^{i\phi} \cos \theta |1\rangle_C, \end{aligned} \quad (4)$$

where $\{|0\rangle_C, |1\rangle_C\}$ is the Charlie's computational basis. Then, the EoA is given as the maximum value of a nonlinear function of two variables, $\bar{S}(\theta, \phi)$,

$$E_A(\theta, \phi) = \max_{\{\theta, \phi\}} \bar{S}(\theta, \phi), \quad (5)$$

where

$$\bar{S}(\theta, \phi) = \sum_i p_i(\theta, \phi) S\left(\frac{\text{Tr}_{BC} [\Pi_i \rho_{ABC} \Pi_i]}{p_i(\theta, \phi)}\right), \quad (6)$$

is the average entropy, $\bar{S}(\theta, \phi) = p_\xi(\theta, \phi) S(\rho_A^\xi) + p_\chi(\theta, \phi) S(\rho_A^\chi)$. The projectors in Eqs. (6) are given by $\Pi_i \equiv \Pi_i(\theta, \phi) = \mathbf{1}_A \otimes \mathbf{1}_B \otimes |i\rangle\langle i|$, with $i = \xi, \chi$, respectively, with the associate probability distribution: $p_i(\theta, \phi) = \text{Tr}_{ABC} [\Pi_i(\theta, \phi) \rho_{ABC} \Pi_i(\theta, \phi)]$.

The optimization problem involved in Eq. (5) is not a trivial task, specially if the matrices that represent the tripartite pure states shared by ABC are dense matrices. Here we use a numerical method to find both the maximum and the minimum values of Eq. (5) for arbitrary pure tripartite states. However, we present in section V the exact analytical results concerning two specific kinds of tripartite entangled states: the GHZ-type and the W-type. These states are represented by sparse matrices allowing analytical results. Nonetheless, before we go through the analytical and numerical results, we present in the next section a quantity that demonstrates to be a helpful tool for distinguishing genuine tripartite entangled states from biseparable and separable tripartite states and, beyond, gives a lower bound to identify GHZ-type.

III. ACTIVATED BIPARTITE ENTANGLEMENT

To account exclusively for the entanglement localized in the pair AB doing local projective measurements in C, the Activated Bipartite Entanglement (ABE) is defined as the maximal difference between the average entropies, $\bar{S}(\varepsilon)$, of the

reduced state ρ_A prior and posterior actuation on C ,

$$\begin{aligned}\Delta_E(\rho_{AB}) &\equiv \max_{\varepsilon} [\bar{S}(\varepsilon_p) - \bar{S}(\varepsilon_a)] \\ &= \max_{\varepsilon_p} \bar{S}(\varepsilon_p) - \min_{\varepsilon_a} \bar{S}(\varepsilon_a),\end{aligned}\quad (7)$$

where ε_a and ε_p , represent the anterior (prior operation on C) and posterior (after operation on C) ensembles of pure state decomposition of $\rho_{AB} = \text{Tr}_C \rho_{ABC}$ and $\rho_{AB}^p \equiv \text{Tr}_C [\sum_i \Pi_i \rho_{ABC} \Pi_i]$. Taking into account Eqs. (2) and (3), the difference given by Eq. (7) can be expressed as the difference between the EoA and the EoF of state ρ_{AB} ,

$$\Delta_E(\rho_{AB}) = E_A(\rho_{AB}) - E_F(\rho_{AB}). \quad (8)$$

In that sense, the ABE, for many copies of a state ρ_{ABC} , quantifies the rate of maximally entangled bipartite states that are successfully activated. In other words, $E_F(\rho_{AB})$ measures the amount of entanglement that already exists between Alice and Bob before Charlie's assistance, while $\Delta_E(\rho_{AB})$ represents the extra amount added to it after the assistance. Note that, since the EoA is the maximum value of the average entropy (given by Eq. (1)) over all pure state decomposition of ρ_{AB} while EoF is the minimum value of the same function over the same decomposition, by construction, the ABE cannot be negative and it is always greater than or equal to zero,

$$\Delta_E(\rho_{AB}) = E_A(\rho_{AB}) - E_F(\rho_{AB}) \geq 0. \quad (9)$$

Therefore $E_F(\rho_{AB})$ is the lower bound of $E_A(\rho_{AB})$.

Here, we argue that the EoA will be always equal to the EoF, $E_A(\rho_{AB}) = E_F(\rho_{AB})$, i.e., $\Delta_E(\rho_{AB}) = 0$, for states belonging to the classes of biseparable and fully separable pure tripartite states [21]. Otherwise, for states with truly tripartite entanglement, such as GHZ-type and W-type, the difference given by Eq. (9) is always positive and different to zero, i.e., $\Delta_E(\rho_{AB}) > 0$. The practical meaning is that there is no Charlie's local measurement capable to concentrate any extra amount of entanglement between Alice and Bob, besides the amount that already exist, if the three parts of the combined system ABC share non-tripartite entanglement. On the other hand, it is always possible to inject additional entanglement between AB acting on C if the state shared by ABC is of GHZ-type or W-type. Thus, Δ_E can be used as a witness to testify if a three-qubit pure state presents truly tripartite entanglement or not.

Besides, the ABE has an upper bound, which means that the total extra amount of entanglement that can be localized by acting on C is limited. It is interesting to note that the upper bound of the ABE has already appeared in the original derivation of the EoA, as given by DiVincenzo *et al.* [10],

$$\Delta_E(\rho_{AB}) \leq S(\rho_{AB}) - |S(\rho_A) - S(\rho_B)|. \quad (10)$$

The upper bound given by Eq. (10) is a helpful tool to retrieve information about the inequivalent class under LOCC (that is, the GHZ class or the W class) a genuine tripartite entangled pure state belongs to [22]. As will be clarified in the next section, the ABE alone distinguishes states between the two inequivalent classes (under LOCC) of authentic tripartite entanglement, that is, it can say alone if the state belongs to the GHZ or the W class.

IV. NUMERICAL RESULTS FOR ARBITRARY STATES

The EoA as well as the EoF defined in the previous sections are examples of optimization problems that can be solved via classical optimization techniques (usually linear or nonlinear programming) or through heuristic methods. In the classical optimization paradigm, it is presumed that solutions exist and are identified through enumeration or differential calculus. Problems are usually set in the form: the multi-variable function $f(x_1, x_2, \dots, x_n)$ we wish to find the maximum (or minimum) is called Objective Function (OF) and it can be constrained to a specific search space.

In our case, the OF is the two-variable function given by Eq. (6), that is

$$\bar{S}(\theta, \phi) = p_\xi(\theta, \phi) S(\rho_A^\xi) + p_\chi(\theta, \phi) S(\rho_A^\chi), \quad (11)$$

where

$$\rho_A^i = \text{Tr}_{BC} \left[\frac{\Pi_i(\theta, \phi) \rho_{ABC} \Pi_i(\theta, \phi)}{p_i(\theta, \phi)} \right]. \quad (12)$$

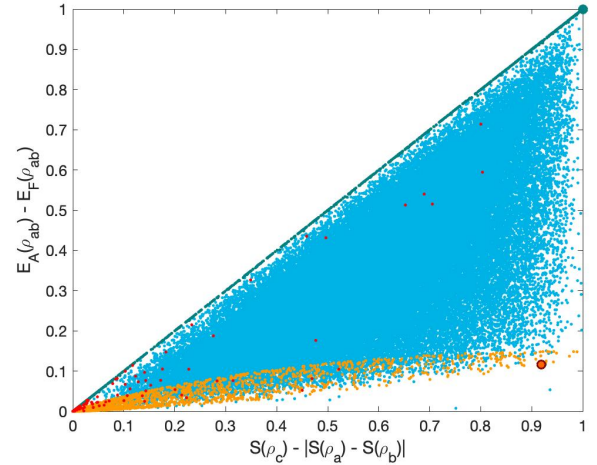


FIG. 1. The (numerically solved) Activated Bipartite Entanglement plotted against its upper bound given by Eq. (10). The single dots in light-blue represent a total of 8×10^4 randomly generated tripartite pure states satisfying the Haar measure. The dots in green over the straight line $E_A(\rho_{AB}) - E_F(\rho_{AB}) = S(\rho_{AB}) - |S(\rho_A) - S(\rho_B)|$ represent a total of 1×10^3 1-parameter GHZ-type of states given by Eq. (15). The dots in orange represent a total of 2×10^3 W-type of states with half of them given by the 3-parameter decomposition expressed by Eq. (17) and the other half formed by the 2-parameter decomposition given by Eq. (18), respectively. The single dots in red represent a total of 1×10^2 arbitrary states given by Eq. (14). The two big dots at coordinates (1,1) (green) and (0.11, 0.9183) (orange) are respectively the usual GHZ and W states given by Eqs. (20) and (25).

The strategy used here to find the extremes of $\bar{S}(\theta, \phi)$ is to perform a numerical search for the roots that satisfy simulta-

neously the following set of nonlinear equations

$$\begin{aligned}\frac{\partial}{\partial\theta}\bar{S}(\theta,\phi) &= 0, \\ \frac{\partial}{\partial\phi}\bar{S}(\theta,\phi) &= 0,\end{aligned}\quad (13)$$

and then seek for the maximum and minimum values of the OF evaluated at the stationary points. To solve numerically the pair given by Eqs. (13) we use a Globally Convergent Method for Systems of Non-Linear Equations with Line Searches and Backtracking described in Ref. [23]. This method has proven to be a suitable optimization technique for our purposes, i.e., to calculate the EoA and EoF of arbitrary pure three-qubit states.

The arbitrary tripartite pure states were randomly generated obeying the Haar measure. In Fig. (1) we plot 8×10^4 of these states (light-blue dots), as quantified by the ABE against its upper bound given by Eq. (10). As we can observe, the 8×10^4 random states scatter all over the allowed area limited by the triangle whose legs are given by the ABE and by the right-hand side of Eq. (10). Calculus of the rank of the associated reduced density matrices ρ_A , ρ_B and ρ_C , shows that the arbitrary states over the triangle area (except for the points at the origin) have $r(\rho_A) = r(\rho_B) = r(\rho_C) = 2$, a characteristic trait only fulfilled by the two inequivalent classes of entanglement, the GHZ-type and the W-type. The points at the origin correspond to all separable and biseparable states – therefore they must have at least one of the ranks equal to 1 (for biseparable states, the rank of one of them is equal to 1 and for completely separable states the three ranks are equal to 1) [6], a result that was prompt satisfied. Thus, the simple fact that the ABE is greater than zero ensures that the corresponding state has genuine tripartite entanglement. To find a way to distinguish the GHZ-type from the W-type using the ABE (and its bound), we study the possible product decomposition the 3-qubit pure states can assume, expecting that some characteristic feature arises. In fact, as we will see, the GHZ-type and the W-type states present distinct features associated with the amount of entanglement of Alice and Bob, assisted by Charlie, which can be seen through the decomposition mentioned and tested via the 3-Tangle.

Another way to describe arbitrary tripartite pure states is through its Generalized Schmidt Decomposition [24, 25],

$$|\psi_3\rangle = \lambda_0|000\rangle + \lambda_1|100\rangle + \lambda_2|101\rangle + \lambda_3|110\rangle + \lambda_4|111\rangle, \quad (14)$$

where $\lambda_i \geq 0$ and $\sum_i \lambda_i^2 = 1$. In Fig. (1) we plot these states (the red dots scattered along the same allowed area) for a 1×10^2 randomly chosen set of parameters. These states encompass all kinds of 3-qubit states, i.e., GHZ-type, W-type, biseparable states and separable states. Three particular kinds of decomposition derived from Eq. (14) help us to understand the behavior of the GHZ-type and W-type under the ABE and its upper bound: (i) the 1-parameter GHZ-type, (ii) the 3-parameter and (iii) the 2-parameter W-type.

The first kind considered here represents states which can

be expressed as the sum of only two product vectors,

$$|\psi_{GHZ}\rangle = \lambda_1|000\rangle + \lambda_2|111\rangle, \quad (15)$$

i.e., represents the 1-parameter GHZ-type (where $\lambda_2 = \sqrt{1 - \lambda_1^2}$). They are depicted in Fig. (1) by the 1×10^3 green dots (generated by randomly choosing the independent parameter λ_1) along the straight line $\Delta_E(\rho_{AB}) = S(\rho_{AB}) - |S(\rho_A) - S(\rho_B)|$. This line represents the saturation of Eq. (10), meaning that for the 1-parameter GHZ-type of states, $\rho_{AB} = |\psi_{GHZ}\rangle\langle\psi_{GHZ}|$, the ABE attained its maximum permitted value

$$\Delta_E(\rho_{AB}) = S(\rho_{AB}), \quad (16)$$

since $S(\rho_{AB}) = S(\rho_A) = S(\rho_B) = S(\rho_C)$ for these specific states. Being a GHZ state, the 1-parameter GHZ-type presents a 3-Tangle [26], greater than zero [6] (except for the trivial cases of $\lambda_1 = 0$ or $\lambda_1 = 1$). Therefore, one of our results (that will be showed through analytical results in the next section) are the following: 1-parameter GHZ-type of states saturate the ABE upper bound.

Beyond the 1-parameter GHZ-type, we consider the 3 and the 2-parameter W-type of states given, respectively, by the following decompositions

$$|\psi_{W3}\rangle = \lambda_0|000\rangle + \lambda_1|100\rangle + \lambda_2|101\rangle + \lambda_3|110\rangle, \quad (17)$$

$$|\psi_{W2}\rangle = \lambda_1|100\rangle + \lambda_2|010\rangle + \lambda_3|001\rangle, \quad (18)$$

where the coefficients in both Eqs. (17) and (18) must satisfy the constraints $\lambda_i \geq 0$ and $\sum_i \lambda_i^2 = 1$. Choosing the three and two independent parameters for each decomposition randomly, it is possible to notice that the W-type of states covers a specific region in Fig. (1) (which is represented by the 2×10^3 dots in orange). The maximum value attained by the ABE for these states is $\Delta_E(\rho_{AB}) \approx 0.15$, which redefines the ABE's upper bound for the W-type,

$$0 \leq \Delta_E(\rho_{AB}^{W\text{-type}}) \leq 0.15, \quad (19)$$

In the next section, we give a precise reason for that to happen. As we will see, the W-type of states live in a parametric surface (depicted in Fig. 3) and what is seen in Fig. (1) is the shadow of this surface in the $\Delta_E(\rho_{AB}) \times S(\rho_{AB}) - |S(\rho_A) - S(\rho_B)|$ plane. As expected, the 3-Tangle values for these 2×10^3 states are all equal to zero.

To conclude our numerical analyses, calculus of the 3-Tangle for the 8×10^4 light-blue dots reveals two important things: (i) the states that present the 3-Tangle equals to zero are all localized in the W-type region while (ii) the dots between the regions defined by the 1-parameter GHZ-type and the 3 and 2-parameters W-type present values greater than zero, a *sine qua non* condition for the identification of GHZ states. Therefore, we conclude that these states are all of GHZ-type and with LOCC they can be converted into 1-parameter GHZ-type. Besides, another important result of this paper is the understand that if the $\Delta_E(\rho_{AB}) > 0.15$ for a particular tripartite pure state, this state pertain to the GHZ class of entanglement.

V. EXACT RESULTS FOR THE GHZ AND W STATES

Fortunately, both the GHZ and W states are represented by sparse matrices and the OFs associated to them are very simple allowing analytical and exact solutions for the set of equations (13) associated to these particular states (even for the 1-parameter GHZ-type and the 2-parameter W-type).

The simplest case, naturally, is given by the well-known GHZ state

$$|GHZ\rangle = \frac{1}{\sqrt{2}} (|000\rangle + |111\rangle), \quad (20)$$

whose average entropy given by Eq. (6) is obtained exactly and depends solely on θ as a Binary Entropy with $p = \cos^2 \theta$,

$$\bar{S}_{|GHZ\rangle}(\theta) = -p \log_2 p - (1-p) \log_2 (1-p). \quad (21)$$

The EoA for the GHZ state is the maximum value of $\bar{S}_{|GHZ\rangle}(\theta)$ given by Eq. (21) which is attained at $\theta = \pi/4$ ($p = 1/2$): $E_A(\rho_{AB}) = \bar{S}_{|GHZ\rangle}(\pi/4) = 1$; the minimum values of $\bar{S}_{|GHZ\rangle}(\theta)$ are reached at $\theta = 0$ and $\theta = \pi/2$ ($p = 1$ or $p = 0$) and they correspond to the EoF for the GHZ state: $E_F(\rho_{AB}) = \bar{S}_{|GHZ\rangle}(0) = \bar{S}_{|GHZ\rangle}(\pi/2) = 0$. Therefore, the optimal basis in which Charlie can maximize his assistance is spanned by the eigenvectors of Pauli's σ_x operator. The basis formed by the eigenvectors of Pauli's σ_z operator minimizes the average entropy, consequently, minimizes his assistance. Since the EoF is always zero for any bi-partition of the GHZ state [27], the ABE is simply equivalent to the EoA: $\Delta_E(\rho_{AB}) = E_A(\rho_{AB}) = 1$. In addition, the GHZ state saturates the upper bound given by Eq. (10)

$$\Delta_E(\rho_{AB}) = S(\rho_{AB}), \quad (22)$$

since $S(\rho_{AB}) = S(\rho_A) = S(\rho_B) = S(\rho_C) = 1$. This can be seen as a characteristic trait concerning the consensual agreement regarding the idea that the GHZ state is the maximally entangled tripartite state, adding one more interesting property to the list of properties which corroborate to this hypothesis. Since the entanglement between any bi-partition of the GHZ state is null before a third part assistance and is maximal (and equal to the entanglement shared initially by the trio ABC) after the assistance, the equality given by Eq. (22) may represent an authentication of the true nature of its tripartite entanglement. In other words, the fact that the GHZ state is the state that provides the best resource in terms of Charlie's assistance that Alice and Bob can get, can be understood as a trait of genuine tripartite entanglement in the sense that, unlike the W state, the GHZ state is not built as the sum of its three bipartite entanglements.

Indeed, every 1-parameter GHZ-type of state given by Eq. (15) presents the same features described above for the special case of the usual GHZ state given by Eq. (20). For instance, the EoF of any bi-partition of these states are always equal to zero. This imply that the ABE and the EoA are always equal to each other, expressing the fact that, if the trio ABC shares a 1-parameter GHZ state, all the entanglement that Alice and Bob can get to eventually perform

some task comes from the Charlie's assistance. Furthermore, $S(\rho_{AB}) = S(\rho_A) = S(\rho_B) = S(\rho_C) = -\lambda_1^2 \log_2(\lambda_1^2) - \lambda_2^2 \log_2(\lambda_2^2)$ (a result that can be easily checked) which implies that the right hand side of Eq. (10) reduces to $S(\rho_{AB})$, i.e., $\Delta_E(\rho_{AB}) = E_A(\rho_{AB}) \leq S(\rho_{AB})$. However, a more interesting feature showed numerically in the last section is the fact that the 1-parameter GHZ-type of states always saturate the ABE's upper bound, i.e.,

$$\Delta_E(\rho_{AB}) = E_A(\rho_{AB}) = S(\rho_{AB}). \quad (23)$$

In fact, Eq. (23) can be analytically verified for the 1-parameter GHZ-type of states. After some exact calculations it is possible to check that the left hand side of Eq. (10) presented (i) a average entropy that does not depend on the relative phase of Charlie's measurement basis, depending solely on θ : $\bar{S}_{|\psi_{GHZ}\rangle}^{(\lambda_1)}(\theta, \phi) = \bar{S}_{|\psi_{GHZ}\rangle}^{(\lambda_1)}(\theta)$, (ii) a maximum value given by $E_A(\rho_{AB}) = -\lambda_1^2 \log_2(\lambda_1^2) - \lambda_2^2 \log_2(\lambda_2^2)$ at $\theta = \pi/4$ and (iii) a minimum values equal to zero at $\theta = 0$ and $\theta = \pi/2$: $E_F = 0$ (see Fig 2).

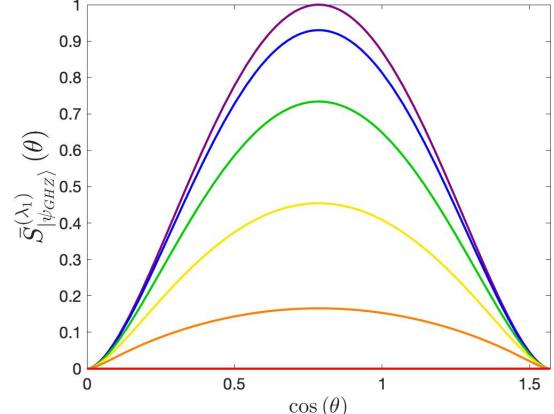


FIG. 2. The average entropy given by Eq. (6) when $\rho_{ABC} = |\psi_{GHZ}\rangle\langle\psi_{GHZ}|$ for different values of λ_1 in Eq. (15). In red, $\lambda_1 = 1$ (or $\lambda_1 = 0$). In orange, $\lambda_1 = 0.9877$. In yellow, $\lambda_1 = 0.9511$. In green, $\lambda_1 = 0.8910$. In blue, $\lambda_1 = 0.8090$. In purple we have the GHZ state given by Eq. (20), i.e., $\lambda_1 = \sqrt{2}/2 = 0.7071$. The average entropies do not depend on the relative phase found in the linear superposition that composes the states in Eqs (4). Varying θ from 0 to $\pi/2$, the maximal values that represent the EoA for the different values of λ_1 considered here, are always reached at $\theta = \pi/4$ (i.e., $\cos(\theta) = \sqrt{2}/2$).

Therefore, the ABE for the 1-parameter GHZ states is given by

$$\Delta_E(\rho_{AB}) = -\lambda_1^2 \log_2(\lambda_1^2) - \lambda_2^2 \log_2(\lambda_2^2), \quad (24)$$

and Eq. (23) holds for these states, showing that Charlie's assistance done in the right basis, concentrates all the entanglement available contained in the GHZ-type state, which is, as expected, dependent on λ_1 parameter.

In Fig. (3) we show the parametric plot with the additional dimension given by the dependent parameter $\lambda_2 = \sqrt{1 - \lambda_1^2}$. As we can observe, since there is only one independent parameter, the 1-parameter GHZ-type of states live in the curved line in blue. The more complete scenario given by the parametric space in Fig. 3 embrace the scenario represented in Fig 1, by the green dots along the line $\Delta_E(\rho_{AB}) = S(\rho_{AB})$.

For the W state,

$$|W\rangle = \frac{1}{\sqrt{3}} (|100\rangle + |010\rangle + |001\rangle), \quad (25)$$

the average entropy given by Eq. (6) is also obtained analytically. Just like the case of 1-parameter GHZ states, the average entropy for the W state depends solely on θ . However, $\bar{S}_{|W\rangle}(\theta)$ is a convex function of the compact parameter $0 \leq \theta \leq \pi/2$, with maximum values at $\theta = 0$ and $\theta = \pi/2$, $E_A(\rho_{AB}) = \bar{S}_{|W\rangle}(0) = \bar{S}_{|W\rangle}(\pi/2) = 0.666$, and minimum value at $\theta = \pi/4$, $E_F(\rho_{AB}) = \bar{S}_{|W\rangle}(\pi/4) = 0.55$. Thus, the bases that maximizes and minimizes the average entropy for the W state are swapped in comparison to the 1-parameter GHZ states which means that for the W state the σ_z basis maximizes and the σ_x basis minimizes the average entropy (the opposite order fo the 1-parameter GHZ states). The ABE is greater than zero, $\Delta_E(\rho_{AB}) = 0.11$, as it should be, but it is far below the upper bound: $\Delta_E(\rho_{AB}) \leq 0,9183$.

We also solved the ABE analytically for the 2-parameter W-type as given by Eq. (18). The parametric equations for that states are also plotted in Fig. (3). We see that GHZ-class and W-class states live in antipodal regions of all the possible 3-qubit pure states.

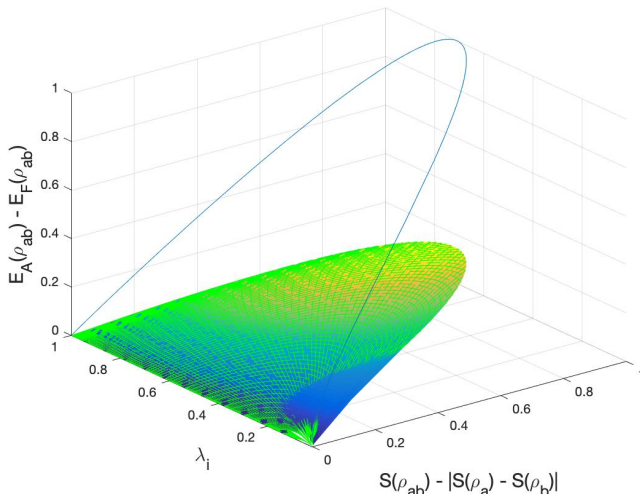


FIG. 3. Parametric curve and parametric surface for both, the 1-parameter GHZ-type and the 2-parameter W-type states, respectively. The parameter λ_i is the independent parameter.

VI. EXPERIMENTAL PROPOSAL WITH LINEAR OPTICAL CIRCUIT

Our experimental proposal is based on the use of internal degrees of freedom of light [18, 19] associated with single photon source produced by SPDC [16]. In particular, we use three degrees of freedom of a single photon to codify qubits, namely propagation path (p), polarization (P), and transverse modes (M). Our tripartite state is described by $|pPM\rangle$.

The computational basis of polarization qubit (Alice) is codified in the H/V basis in such way we have $|H\rangle \equiv |0\rangle_A$ and $|V\rangle \equiv |1\rangle_A$. For the transverse mode qubit (Bob), we propose the use of first order Hermitian-Gaussian mode HG_{01} , labeled as h due the horizontal dumbbell shape, and HG_{10} , labeled as v considering the vertical dumbbell shape. The transverse modes h and v form an orthonormal basis and we can codify the qubit as $|h\rangle \equiv |0\rangle_B$ and $|v\rangle \equiv |1\rangle_B$. Finally, to codify path qubit (Charlie) we used two parallel path, labeled up (u) and down (d), and we have $|u\rangle \equiv |0\rangle_C$ and $|d\rangle \equiv |1\rangle_C$. Then, defining the order of qubits as Charlie, Alice and Bob ($|C\rangle \otimes |A\rangle \otimes |B\rangle$) a photon propagating in the path u , with polarization H , transverse mode h has its tripartite state defined as $|uHh\rangle \equiv |000\rangle$, and, consequently, $|dVv\rangle \equiv |111\rangle$.

The preparation of tripartite states of three internal degrees of freedom of a photon follows the proposal of Ref.[19] associated to single photon sources produced by SPDC. Polarized single photons can be prepared with h/v transverse modes and have their path controlled. Then, a general tripartite state can be prepared. Let us show the optical circuits and their simulation for GHZ and W state.

A. GHZ state

The optical circuit for preparation of a single photon in GHZ-type state defined in Eq. (15) is presented in Figure 4. A Spontaneous Parametric Down Conversion (SPDC) source composed by laser of frequency ω_p pumping a nonlinear crystal (NLC) produces twin photons Signal, with frequency ω_s , used for GHZ preparation, and Idler, with frequency ω_i , used for trig the measurement apparatus, that obey the phase matching condition and $\omega_p = \omega_s + \omega_i$.

The signal passes through a S-Wave Plate (SWP) in order to prepare radial polarization, that corresponds to the spin-orbit entangled state of the system AB . In PBS_1 a polarization projective measurement is performed and we have the state $|\Psi_1\rangle = |Hh\rangle \equiv |00\rangle_{AB}$. This is a simple and very efficient way to prepare the initial state.

The path qubit can be prepared by a variable beam splitter that can be performed by the Half Wave Plate with its fast axis with an angle θ with the horizontal and a polarized beam splitter. HWP_θ transforms the polarization and we have

$$|\Psi_2\rangle = |h\rangle \otimes [\cos(2\theta) |H\rangle + \sin(2\theta) |V\rangle]. \quad (26)$$

The PBS_2 projects H-polarization in path u and V-polarization in path d . Then, we have a tripartite state prepared as

$$|\Psi_3\rangle = \cos(2\theta) |uHh\rangle + \sin(2\theta) |dVv\rangle. \quad (27)$$

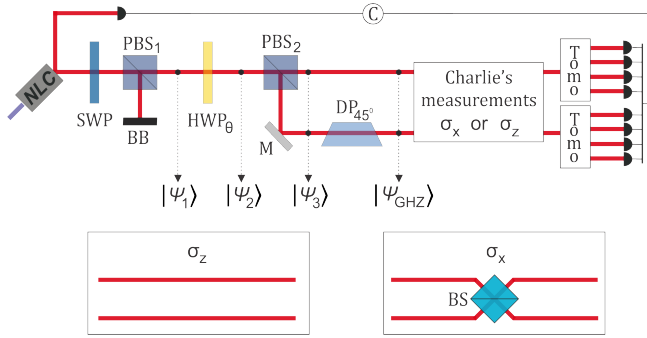


FIG. 4. Experimental setup for GHZ-like states. NLC: non linear crystal, SWP: S-wave plate to produce spin-orbit nonseparable modes, PBS: Polarized Beam Splitter, HWP_θ : half wave plate with its fast axis with an angle θ with horizontal, DP_{45° : Dove prism with its base rotated of 45° with respect the horizontal, TOMO: tomography circuit for spin-orbit states as proposed in Ref.[28]. The tomography outputs in both paths are detected by photocounters detectors that are triggered by coincidence with the detection of Idler. BS: 50/50 non polarized Beam Splitter.

Finally, the Dove prism (DP) performs the transformation $|h\rangle \rightarrow |v\rangle$ in transverse mode in the path d and Signal presents the state

$$|\Psi_{GHZ}\rangle = \cos(2\theta) |uHh\rangle + \sin(2\theta) |dVv\rangle, \quad (28)$$

where $\lambda_1 = \cos(2\theta)$ and $\lambda_2 = \sin(2\theta)$. The preparation is complete. Lets discuss the measurement. At the end of each path, we have a spin-orbit state tomography circuit, as presented in [28]. With the tomography circuit, we will reconstruct the reduced density matrix ρ_{AB} . Before the tomography, Charlie needs to perform measurements of σ_Z and σ_X . For σ_Z , both paths are free and the click in the paths u or d give the result 0 or 1 for this measure. For σ_X , path u and d are sent to a Beam Splitter (BS) [18] and the BS's output goes to tomography circuit.

We simulate the preparation and measurement of GHZ-type states by using Jones Matrix formalism [29]. Our experimental proposal was designed to give as output the reduced density matrix ρ_{AB} of spin-orbit states multiplied by the corresponding weight that depends on λ_1 and λ_2 for GHZ-type states. The matrix obtained is used to calculated ABE ($E_A(\rho_{AB}) - E_F(\rho_{AB})$). We introduced in the simulation error of $\pm 1^\circ$ in the angle θ of the HWP that defines the weigh λ_1 and λ_2 in order to emulate experimental errors. Figure 5 presents the measurement results for $\lambda_1 = \lambda_2 = \frac{1}{\sqrt{2}}$. Fig.5-a) shows the obtained matrix for Charlie's measurement of σ_Z resulting 0, Fig.5-b) resulting 1. Fig.5-c) shows the results of ρ_{AB} for Charlie's measurement of σ_X resulting 0 and Fig.5-d) resulting 1. The partial trace is obtained by the convex sum of the matrix of paths 0 and 1 with the respective weight. The obtained matrices by the optical circuit simulation are in excellent agreement with theoretical expectation presenting fidelity of 0.97, 0.99, 0.99, and 0.99, respectively. For this case we obtain $E_A(\rho_{AB}) - E_F(\rho_{AB}) = 0.9992$, that presenting an error of less than 0.01% with respect the theoretical expectation.

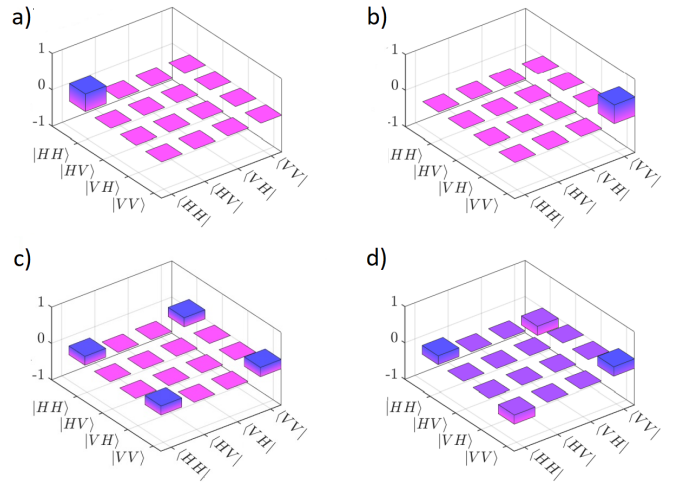


FIG. 5. Results of the tomography for GHZ-type states after Charlie's measurement of a) σ_Z resulting 0, b) σ_Z resulting 1, c) σ_X resulting 0, and d) σ_X resulting 1. The results are the density matrix of the reduced state AB (spin-orbit state) multiplied by the corresponding weigh that depends on λ_1, λ_2 , in this case $\frac{1}{2}$.

B. W state

Now, let us present the experimental proposal for a study of W-type state given by Eq.(18). Figure 6 presents the optical circuit for preparation and measurements. The circuit is the same one for GHZ-type until the preparation of state $|\Psi_3\rangle$, given by Eq.27. Here we use an angle α for the first HWP for path preparation.

A photon in the path d passes through a HWP_{45° and transforms its polarization as $|V\rangle \rightarrow |H\rangle$ and this part of the state is in accordance of the first term of Eq.18, $\lambda_1 |100\rangle$, where $\lambda_1 = \sin(2\alpha)$ and $|100\rangle \equiv |dHh\rangle$. The other two terms are associate to path u , and we can write $|0\rangle_C \otimes (\lambda_2 |10\rangle + \lambda_3 |01\rangle)$. The terms in parentheses are an unbalanced entangled state in the spin-orbit degree of freedom of light with weigh λ_2 and λ_3 . It can be prepared by a C-NOT using polarization as control qubit. The HWP_β will transforms

$$\cos(2\alpha) |Hh\rangle \rightarrow \cos(2\alpha) [\cos(2\beta) |H\rangle + \sin(2\beta) |V\rangle]. \quad (29)$$

The V-polarization is reflected by PBS_3 and is deviated to the PBS_4 and we can write

$$|\Psi_4\rangle = \cos(2\alpha) \cos(2\beta) |uHh\rangle + \cos(2\alpha) \sin(2\beta) |uVh\rangle + \sin(2\alpha) |dHh\rangle. \quad (30)$$

The H-polarization is transmitted in PBS_3 , passes through a Dove Prism (DP) that transforms transverse mode as $|h\rangle \rightarrow |v\rangle$ leading us to

$$|\Psi_5\rangle = \cos(2\alpha) \cos(2\beta) |uHv\rangle + \cos(2\alpha) \sin(2\beta) |uVh\rangle + \sin(2\alpha) |dHh\rangle, \quad (31)$$

and is also deviated also for PBS_4 where is aligned with the other arm of the C-NOT in the path u . Then, finally, we have

$$|\Psi_W\rangle = \sin(2\alpha)|dHh\rangle + \cos(2\alpha)\cos(2\beta)|uHv\rangle + \cos(2\alpha)\sin(2\beta)|uVh\rangle. \quad (32)$$

Taking into account our codification and by comparing with Eq.18, we identify $\lambda_2 = \cos(2\alpha)\cos(2\beta)$ and $\lambda_3 = \cos(2\alpha)\sin(2\beta)$. Here, the preparation is complete.

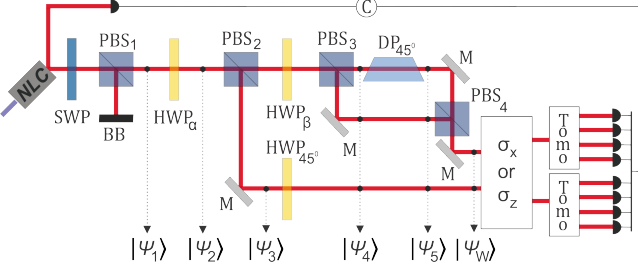


FIG. 6. Experimental setup for W-like state preparation. NLC: non linear crystal, SWP: S-wave plate to produce spin-orbit nonseparable modes, PBS: Polarized Beam Splitter, HWP $_{\phi}$: half wave plate with its fast axis with an angle $\phi = \alpha, \beta, 45^\circ$ with the horizontal, DP $_{45^\circ}$: Dove prism with its base rotated of 45° with respect the horizontal, TOMO: tomography circuit for spin-orbit states as proposed in Ref.[28]. The tomography outputs in both paths are detected by photocounters detectors that are triggered by coincidence with the detection of Idler.

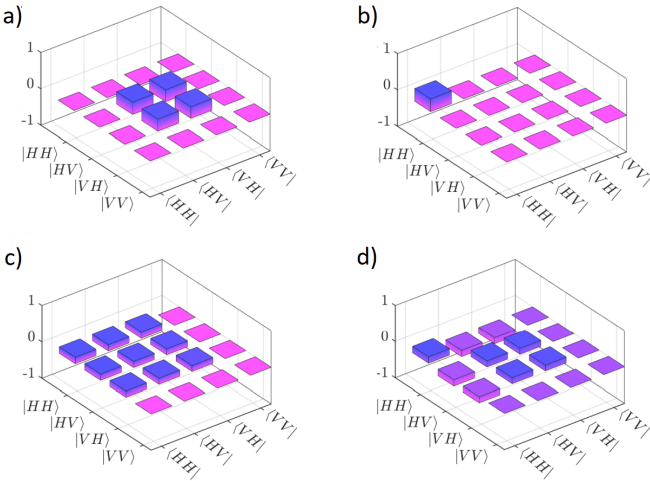


FIG. 7. Results of the tomography for W-type states after Charlie's measurement of a) σ_z resulting 0, b) σ_z resulting 1, c) σ_x resulting 0, and d) σ_x resulting 1. The results are the density matrix of the reduced state AB (spin-orbit state) multiplied by the corresponding weigh that depends on λ_1, λ_2 , and λ_3 , in this case $\frac{1}{3}$.

The measurement circuit is the same used for GHZ-type states. The simulation of preparation and measurement of W-type states by using Jones Matrix formalism [29] follows

the same steps presented for GHZ states. Figure 7 presents the measurement results for $\lambda_1 = \lambda_2 = \lambda_3 = \frac{1}{\sqrt{3}}$. Fig.7-a) and b) show the results of the tomography of the spin-orbit state for Charlie's measurement of σ_z resulting 0 and 1, respectively. Fig.7-c) shows the results of the tomography of the spin-orbit state for Charlie's measurement of σ_x resulting 0 and Fig.7-d) resulting 1. Here we also observed an excellent agreement with theoretical expectation. The fidelity are, respectively, 0.99, 0.99, 0.99, and 0.99. We obtain $E_A(\rho_{AB}) - E_F(\rho_{AB}) = 0.1201$, that presents an error of 3% with respect the theoretical expectation.

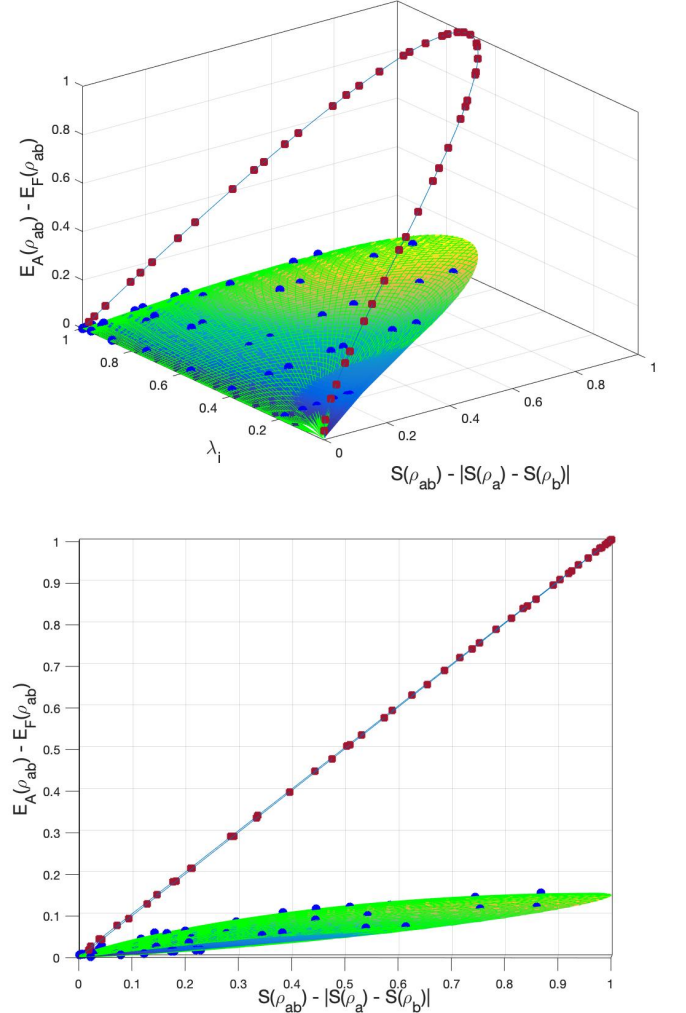


FIG. 8. Top: Curve for GHZ and surface for W type states. Bottom: $E_F(\rho_{AB}) \times S(\rho_{AB}) - |S(\rho_A) - S(\rho_B)|$. Dots are results for optical circuit simulation.

C. Results for optical circuit simulation

By varying θ in the GHZ circuit and, in the same way, α and β in the W state circuit we can perform the simulation of a wide classes of GHZ and W states and use distributed

entanglement classification and compare with the theoretical results presented in Figure 3. Results are presented in Figure 8. The dots represent results obtained by simulation of the optical circuit.

For the GHZ-type states the simulated results appear as squares (purple online) whose dimensions are related to error from the angle θ . As can be seen the Figure 8 (top), the results are very close to the theoretical curve for GHZ-type state.

For W-type states we have spheres (blue online) representing the results for the simulation of optical circuit. They are very well distributed in the expected theoretical surface (Figure 8 - top).

Figure 8 (bottom) presents $E_A(\rho_{AB}) - E_F(\rho_{AB})$ as function of $S(\rho_{AB}) - |S(\rho_A) - S(\rho_B)|$. This is the case evaluated by numerical simulation in Figure 1. The agreement of the simulation of the optical circuit is remarkable.

VII. CONCLUSIONS

In this paper, we propose a way to determine if the states of three-qubit systems present a genuine tripartite entanglement or not via the Activated Bipartite Entanglement (ABE), which is defined by the difference between the EoA and the EoF of the pure state considered. When applied to pure states of three-qubit systems, this approach reveals that if the state has got a genuine tripartite entanglement, the ABE is neces-

sarily greater than zero and, instead, if the state has not got a genuine tripartite entanglement, i.e., if the state is totally or partially separable, the ABE is necessarily equal to zero. We should remark that, as we have only considered projective operations on C , it resulted in the ABE being defined in terms of the EoA and EoF. We could extend the formalism to general POVM, and it would give similar results in terms of the Localizable Entanglement [30], instead. However, this approach would be more difficult to calculate and to experimentally implement. Besides, it would not bring any additional insight.

In addition we presented an experimental proposal of measurement of ABE by using non linear circuit to prepare tripartite states codifying qubits in internal degrees of freedom of a single photon. We designed optical circuits to prepare GHZ and W states and perform all measurements. Simulations of the optical circuits show an excellent agreement with theory.

ACKNOWLEDGMENTS

We would like to thank financial support from the Brazilian funding agencies Conselho Nacional de Desenvolvimento Científico e Tecnológico (CNPq), through the Brazilian National Institute for Science and Technology of Quantum Information (INCT-IQ) Fundação Carlos Chagas Filho de Amparo à Pesquisa do Estado do Rio de Janeiro (FAPERJ), Coordenação de Aperfeiçoamento de Pessoal de Nível Superior (CAPES)..

[1] F. E.S. Steinhoff and M. C. de Oliveira. Families of bipartite states classifiable by the positive partial transposition criterion. *Quantum Information and Computation*, 10:525–538, 5 2010. ISSN 15337146. doi:10.26421/QIC10.5-6-10.

[2] Marcos C. de Oliveira. Characterization and quantification of symmetric gaussian-state entanglement through a local classicality criterion. *Phys. Rev. A*, 72:012317, Jul 2005. doi: 10.1103/PhysRevA.72.012317. URL <https://link.aps.org/doi/10.1103/PhysRevA.72.012317>.

[3] Thiago R. de Oliveira, Gustavo Rigolin, Marcos C. de Oliveira, and Eduardo Miranda. Multipartite entanglement signature of quantum phase transitions. *Phys. Rev. Lett.*, 97: 170401, Oct 2006. doi:10.1103/PhysRevLett.97.170401. URL <https://link.aps.org/doi/10.1103/PhysRevLett.97.170401>.

[4] Ryszard Horodecki, Paweł Horodecki, Michał Horodecki, and Karol Horodecki. Quantum entanglement. *Reviews of modern physics*, 81(2):865, 2009.

[5] Ingemar Bengtsson and Karol Życzkowski. *Geometry of Quantum States: An Introduction to Quantum Entanglement*. Cambridge University Press, 2 edition, 2017. doi: 10.1017/9781139207010.

[6] W. Dür, G. Vidal, and J. I. Cirac. Three qubits can be entangled in two inequivalent ways. *Phys. Rev. A*, 62:062314, Nov 2000. doi:10.1103/PhysRevA.62.062314. URL <https://link.aps.org/doi/10.1103/PhysRevA.62.062314>.

[7] Frank Verstraete, Jeroen Dehaene, and Bart De Moor. Normal forms and entanglement measures for multipartite quantum states. *Phys. Rev. A*, 68:012103, Jul 2003. doi: 10.1103/PhysRevA.68.012103. URL <https://link.aps.org/doi/10.1103/PhysRevA.68.012103>.

[8] Gilad Gour and Nolan R. Wallach. All maximally entangled four-qubit states. *Journal of Mathematical Physics*, 51(11):112201, 2010. doi:10.1063/1.3511477. URL <https://doi.org/10.1063/1.3511477>.

[9] Gilad Gour and Nolan R. Wallach. Classification of multipartite entanglement of all finite dimensionality. *Phys. Rev. Lett.*, 111:060502, Aug 2013. doi:10.1103/PhysRevLett.111.060502. URL <https://link.aps.org/doi/10.1103/PhysRevLett.111.060502>.

[10] David P DiVincenzo, Christopher A Fuchs, Hideo Mabuchi, John A Smolin, Ashish Thapliyal, and Armin Uhlmann. Entanglement of assistance. In *NASA International Conference on Quantum Computing and Quantum Communications*, pages 247–257. Springer, 1998.

[11] William K Wootters. Entanglement of formation of an arbitrary state of two qubits. *Physical Review Letters*, 80(10):2245, 1998.

[12] Jian-Wei Pan, Zeng-Bing Chen, Chao-Yang Lu, Harald Weinfurter, Anton Zeilinger, and Marek Żukowski. Multiphoton entanglement and interferometry. *Reviews of Modern Physics*, 84(2):777, 2012.

[13] M. P. Almeida, F. de Melo, M. Hor-Meyll, A. Salles, S. P. Walborn, P. H. Souto Ribeiro, and L. Davidovich. Environment-induced sudden death of entanglement. *Science*, 316(5824):579–582, 2007. doi: 10.1126/science.1139892. URL <https://www.science.org/abs/10.1126/science.1139892>.

[14] Cristian Antonelli, Mark Shtai, and Misha Brodsky. Sudden death of entanglement induced by polarization mode dispersion. *Physical review letters*, 106(8):080404, 2011.

[15] Ashutosh Singh, Siva Pradyumna, A. R. P. Rau, and Urbasi Sinha. Manipulation of entanglement sudden death in an all-optical setup. *J. Opt. Soc. Am. B*, 34(3): 681–690, Mar 2017. doi:10.1364/JOSAB.34.000681. URL <http://www.osapublishing.org/josab/abstract.cfm?URI=josab-34-3-681>.

[16] Gonzalo Carvacho, Francesco Graffitti, Vincenzo D’Ambrosio, Beatrix C. Hiesmayr, and Fabio Sciarrino. Experimental investigation on the geometry of ghz states. *Sci. Rep.*, 7:13265, Oct 2017. doi:10.1038/s41598-017-13124-6. URL <https://www.ncbi.nlm.nih.gov/pmc/articles/PMC5643536/>.

[17] Xi-Lin Wang, Yi-Han Luo, He-Liang Huang, Ming-Cheng Chen, Zu-En Su, Chang Liu, Chao Chen, Wei Li, Yu-Qiang Fang, Xiao Jiang, Jun Zhang, Li Li, Nai-Le Liu, Chao-Yang Lu, and Jian-Wei Pan. 18-qubit entanglement with six photons’ three degrees of freedom. *Phys. Rev. Lett.*, 120: 260502, Jun 2018. doi:10.1103/PhysRevLett.120.260502. URL <https://link.aps.org/doi/10.1103/PhysRevLett.120.260502>.

[18] W. F. Balthazar, C. E. R. Souza, D. P. Caetano, E. F. Galvao, J. A. O. Huguenin, and A. Z. Khoury. Tripartite nonseparability in classical optics. *Opt. Lett.*, 41(24): 5797–5800, Dec 2016. doi:10.1364/OL.41.005797. URL <http://www.osapublishing.org/ol/abstract.cfm?URI=ol-41-24-5797>.

[19] W. F. Balthazar and J. A. O. Huguenin. Conditional operation using three degrees of freedom of a laser beam for application in quantum information. *J. Opt. Soc. Am. B*, 33(8):1649–1654, Aug 2016. doi:10.1364/JOSAB.33.001649. URL <http://www.osapublishing.org/josab/abstract.cfm?URI=josab-33-8-1649>.

[20] Charles H Bennett, Herbert J Bernstein, Sandu Popescu, and Benjamin Schumacher. Concentrating partial entanglement by local operations. *Physical Review A*, 53(4):2046, 1996.

[21] Note1. To justify this point, let us analyse case by case separately. First, let us examine the cases where $\Delta_E = 0$. To begin with, for the trivial case of a pure tripartite separable state ($\rho_{ABC} = \rho_A \otimes \rho_B \otimes \rho_C$) both EoA and EoF are equal to zero because, in this particular case, for the combined state to be pure each part A, B and C must be also pure which implies that $S(\rho_A) = S(\rho_B) = S(\rho_C) = S(\rho_{AB}) = 0$. Since $E_F(\rho_{AB}) \leq E_A(\rho_{AB}) \leq \min\{S(\rho_A), S(\rho_B)\}$ (see Ref. [10]) and since the EoF assumes the simple form $E_F(\rho_{AB}) = S(\rho_A)$ for the pure state $\rho_{AB} = \rho_A \otimes \rho_B$, we see that $E_A(\rho_{AB}) = E_F(\rho_{AB}) = 0$. Now, for biseparable states we have three distinct scenarios. The first one is the case where the part AB is not entangled with C ($\rho_{ABC} = \rho_{AB} \otimes \rho_C$). In this case, since the tripartite state ρ_{ABC} is pure, the reduced states ρ_{AB} and $\rho_C = \text{Tr}_{AB} \rho_{ABC}$ must be also pure, consequently $S(\rho_{AB}) = S(\rho_C) = 0$, and thereby $S(\rho_A) = S(\rho_B) = E_F(\rho_{AB}) = E_A(\rho_{AB})$ (with $0 \leq S(\rho_A) \leq 1$ depending on the amount of entanglement between AB). Mathematically speaking, the objective function given by Eq. (6) is constant and does not depend on any basis chosen by Charlie to do his measurements nor any optimization over pure ensemble decomposition. The other two scenarios are the following: the system A is not entangled with BC ($\rho_{ABC} = \rho_A \otimes \rho_{BC}$) or the system B is not entangled with AC ($\rho_{ABC} = \rho_{AC} \otimes \rho_B$). In both cases, Charlie is unable to help Alice and Bob because they are initially disentangled from each other and there is no projective measurement upon Charlie’s qubit that would produce any entanglement between AB. Moreover, in both cases $S(\rho_A) = 0$, then, $E_A(\rho_{AB}) = E_F(\rho_{AB}) = 0$.

[22] Note2. For biseparable and fully separable states, the right hand side of Eq. (10) is always equal to zero. Note that, if C is not entangled to AB we have $S(\rho_{AB}) = 0$ and $S(\rho_A) = S(\rho_B)$, then $E_A(\rho_{AB}) - E_F(\rho_{AB}) \leq 0$; if B is not entangled with the pair AC we have $S(\rho_{AC}) = S(\rho_B) = 0$, $S(\rho_A) = S(\rho_C) = S(\rho_{AB})$ and again the ABE’s upper bound is equal to zero; similarly, if A is not entangled to BC then $S(\rho_{BC}) = S(\rho_A) = 0$ and $S(\rho_B) = S(\rho_C) = S(\rho_{AB})$ which leads to the same conclusion. For the trivial case where the parts A, B and C are completely disentangled from each other, $S(\rho_A) = S(\rho_B) = S(\rho_C) = S(\rho_{AB}) = 0$. Since the ABE cannot be negative by construction, we again reach to the same conclusion as before, i.e., whenever the entanglement between the combined state ABC is not tripartite, $\Delta_E(\rho_{AB}) = 0$.

[23] William H Press, William T Vetterling, Saul A Teukolsky, and Brian P Flannery. *Numerical recipes*, volume 818. Cambridge university press Cambridge, 1986.

[24] Antonio Acín, A Andrianov, L Costa, E Jané, JI Latorre, and Rolf Tarrach. Generalized schmidt decomposition and classification of three-quantum-bit states. *Physical Review Letters*, 85(7):1560, 2000.

[25] Antonio Acín, Dagmar Bruß, Maciej Lewenstein, and Anna Sanpera. Classification of mixed three-qubit states. *Physical Review Letters*, 87(4):040401, 2001.

[26] Valerie Coffman, Joydip Kundu, and William K. Wootters. Distributed entanglement. *Phys. Rev. A*, 61:052306, Apr 2000. doi:10.1103/PhysRevA.61.052306. URL <https://link.aps.org/doi/10.1103/PhysRevA.61.052306>.

[27] Note3. This is due to the fact that the GHZ state is very fragile under particle losses, implying that if we trace out one of the three qubits that forms it the remaining bipartite state is completely unentangled.

[28] W. F. Balthazar, D. G. Braga, V. S. Lamego, M. H. M Passos, and J. A. O. Huguenin. Spin-orbit x states. *Phys. Rev. A*, 103: 022411, Feb 2021. doi:10.1103/PhysRevA.103.022411. URL <https://link.aps.org/doi/10.1103/PhysRevA.103.022411>.

[29] R. Clark Jones. A new calculus for the treatment of optical systems. description and discussion of the calculus. *J. Opt. Soc. Am.*, 31(7):488–493, Jul 1941. doi:10.1364/JOSA.31.000488. URL <http://www.osapublishing.org/abstract.cfm?URI=josa-31-7-488>.

[30] M. Popp, F. Verstraete, M. A. Martín-Delgado, and J. I. Cirac. Localizable entanglement. *Phys. Rev. A*, 71:042306, Apr 2005. doi:10.1103/PhysRevA.71.042306. URL <https://link.aps.org/doi/10.1103/PhysRevA.71.042306>.